



Synthesis, crystal structure, thermal behavior, and fluorescence property of lanthanide complexes based on 2,6-dimethylbenzoic acid and 1,10-phenanthroline

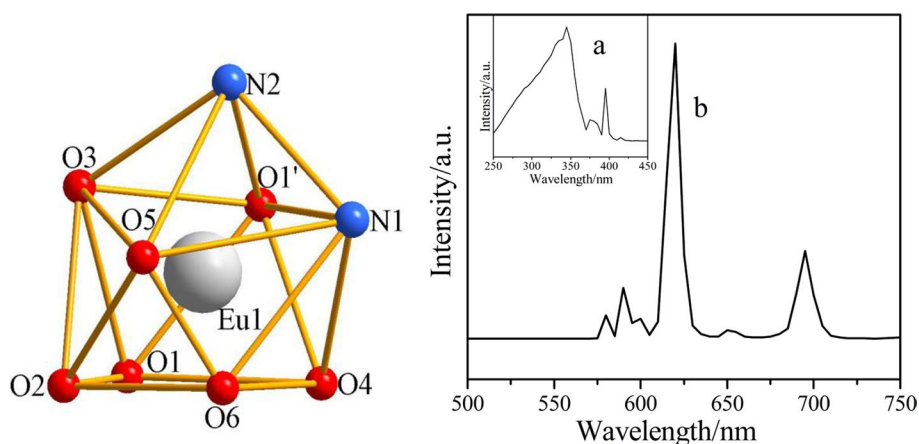
Xin-Xin Wang¹ · Ning Ren² · Yuan-Yuan Ma¹ · Li-Na Geng¹ · Jian-Jun Zhang¹

Received: 5 January 2022 / Accepted: 1 April 2022 / Published online: 14 May 2022
© Institute of Chemistry, Slovak Academy of Sciences 2022

Abstract

Three dinuclear lanthanide complexes were prepared using 2,6-dimethylbenzoic acid and 1,10-phenanthroline as main ligand and auxiliary ligand, namely: [Eu(2,6-DMBA)₃(phen)]₂(1), [Gd(2,6-DMBA)₃(phen)]₂·1.5H₂O(2) and [Tb(2,6-DMBA)₃(phen)]₂·2.5H₂O(3) (2,6-DMBA = 2,6-dimethylbenzoate; phen = 1,10-phenanthroline) and characterized by Raman spectroscopy, infrared spectroscopy, single crystal X-ray diffraction, elemental analysis and thermogravimetric analysis. Single-crystal X-ray diffraction shows that the three complexes were centered on 9 coordination Ln(III) ions and form a single hat tetragonal inverse prism geometry with surrounding nitrogen and oxygen atoms. The adjacent structural units form a 1D chain structure through C–H···O hydrogen bond interaction. TG-DSC/FTIR was used to study the thermal decomposition mechanism of the complexes and the main components of gases escaping during the decomposition process. Solid-state fluorescence studies showed that complexes 1 and 3 emitted strong red and green light, respectively.

Graphical abstract



Keywords Lanthanide complexes · Crystal structure · Thermal analysis · Luminescence property

✉ Ning Ren
ningren9@163.com

✉ Jian-Jun Zhang
jjzhang6@126.com

¹ Testing and Analysis Center, Hebei Normal University, Shijiazhuang 050024, People's Republic of China

² College of Chemical Engineering and Material, Hebei Key Laboratory of Heterocyclic Compounds, Handan University, Handan 056005, People's Republic of China

Introduction

Lanthanide complexes have become a research hotspot for their unique structure and excellent luminescent intensity (Kong et al. 2013; Sun et al. 2020). In addition, more and more attention has been paid to its applications in magnetic materials (Dobies Návía et al. 2018), luminescent material

(Shi et al. 2021), catalyze (Qi et al. 2019), cell imaging material (Kobyłka et al. 2020), biology (Bai et al. 2021). According to the theory of soft and hard acid–base, lanthanide ions, as hard acids, have strong affinity with hard donors containing oxygen and nitrogen atoms (Su et al. 2012). The results show that the complexes with two ligands not only have more stable structures (Kariaka et al. 2016) but also enhance their fluorescence and biological properties (Zapała et al. 2018). Therefore, oxygen-containing aromatic carboxylic acids and nitrogen-containing heterocyclic ligands were the first choice for lanthanide complexes (Ji et al. 2021). The –COOH group in the aromatic carboxylic acid ligand has many binding sites, which not only meets the requirement of high coordination number of rare-earth ions but also can be coordinated by a variety of coordination modes. It was conducive to the construction of novel complexes (Zhang et al. 2021; Xiong et al. 2021). In addition, oxygen atoms in carboxylic acid ligands were easy to form hydrogen bonds with adjacent structural units, which makes the structure of the complexes more stable. The addition of nitrogen-containing heterocyclic ligands can not only meet the requirements of high-coordination number, but also improve the rigidity and stability of the complexes (Zong et al. 2015). Lanthanide ions have weak absorption of light due to the prohibition of f-f electron transition. Organic nitrogen-containing ligands can be used as "antennas" to transfer the absorbed light energy to lanthanide ions. It can promote the transfer of electrons between orbits (Ahmed et al. 2010; Xu et al. 2020) and make it has good luminous performance. This was the theory of "antenna effect" (Guo et al. 2021; Pham et al. 2021). Meanwhile, long fluorescence lifetime, narrow emission peak, and high intensity were also the advantages of lanthanide organic complexes (Zhao et al. 2021). The thermal stability and decomposition mechanism of complexes have become the point of chemists and physicists (Nascimento et al. 2019). TG-DSC/FTIR can be applied to detect the thermal behavior of the complexes at different temperatures and provide useful information for the structures of the complexes (Chesnokov et al. 2018; Zhou et al. 2021). Meanwhile, the thermal decomposition mechanism of complexes also provides an important reference for the synthesis of functional materials with certain thermal stability (Ren et al. 2020; Wang and Zhang 2020; Wang et al. 2016). In recent years, people have carried out in-depth research on organic ligands containing nitrogen and oxygen atoms and having many functions. For example, some lanthanide complexes constructed by aromatic carboxylic acids and nitrogen-containing ligands have been reported in our research group, and a series of characterization and properties of these complexes have been studied. The selected aromatic carboxylic acids were mainly benzoic acid, which was mainly because the oxygen atoms on the carboxylic group have strong affinity and various coordination modes with lanthanide ions.

Nitrogen-containing heterocyclic ligands were mainly o-phenanthroline and pyridine, such as 2,2':6',2''-tripyridine, 5,5'-dimethyl-2,2''-bipyridine and 4,4'-bipyridine, etc. (Du et al. 2021; Zhao et al. 2018). Their large conjugated structures can not only enhance the stability of complexes but also form multi-dimensional supramolecular structures. Therefore, the synthesized complexes have potential applications in sensors, safety devices, and biological imaging (Di et al. 2019; Yang et al. 2017). In this paper, we selected 2,6-dimethylbenzoic acid and 1,10-phenanthroline as ligands to synthesize three lanthanide complexes, namely: [Eu(2,6-DMBA)₃(phen)]₂(1), [Gd(2,6-DMBA)₃(phen)]₂·1.5H₂O(2) and [Tb(2,6-DMBA)₃(phen)]₂·2.5H₂O(3) were synthesized with 2,6-DMBA as acidic ligand, phen as neutral ligand and Ln(NO₃)₃·6(H₂O) as a central ion. The complexes were characterized by elemental analysis, R and IR spectroscopy, and single-crystal X-ray diffraction. The thermal decomposition process and escaping gas of the complexes were studied by TG-DSC and FTIR. The fluorescence properties of solid-state complexes were studied.

Experimental

Materials and reagents

The reagents and drugs used in this study were of high purity and can be used without further purification.

Instruments and experimental conditions

The content of C, H, and N were determined by a Vario EL cube element analyzer. The single-crystal data of the complexes were collected by smart-1000 (Bruker AXS) single-crystal diffractometer at room temperature. The single-crystal data of the complexes were collected on a Smart-1000 single-crystal diffractometer, the emission source was Mo-K α ($\lambda = 0.71073 \text{ \AA}$) monochromatized by graphite. At the same time, the obtained data were improved and refined by SHELXS-97 program, in which the direct method was used for the resolution of non-hydrogen atom, and the total matrix least square method was used for the refinement of its coordinates and anisotropy. The disordered aqueous solvents contained in complexes 2 and 3 were solved using the SQUEEZE program in Platon software (Sheldrick et al. 2015; Boutar et al. 2019). The full matrix least square method was used for refinement. The Raman spectra of complexes and ligands were recorded with BRUKER VERTEX-70FTIR-RAMAN II and an excitation power of 300 mW. The infrared spectra of complexes and ligands in the range of 4000–400 cm⁻¹ were determined by KBr tablet pressing method on BRUKERTENSOR27 Fourier transform infrared spectrometer. The TG, DTG, DSC, and FTIR

analysis of the complexes were measured by NETZSCH STA 449 F3 synchronous thermal analyzer and BRUKER TENSOR27 Fourier transform infrared spectrometer in the simulated atmospheric atmosphere. The fluorescence spectra and lifetime of the complexes were measured by the FS5 fluorescence spectrometer.

Synthesis

0.6 mmol(0.0901 g) of 2,6-DMBA acidic ligand and 0.2 mmol(0.0376 g) of phen neutral ligand were dissolved in 7 mL of 95% ethanol solution, stir and adjust the pH value to 5.4–6.7 with 1 mol/L NaOH solution. Then dissolve 0.2 mmol(0.0892 g, 0.0902 g, 0.08700 g) Ln(NO₃)₃·6(H₂O) in 3 mL distilled water, drop the ligand solution into the stirring lanthanide nitrate solution, and stir for 6–8 h. Stand for 12 h, filter, put the filtered liquid into the beaker, and stand for one week to obtain the crystal. Scheme 1 was the synthesis scheme of complex 1.

Results and discussion

Composition of complexes

Table 1 lists the content of element (C, H, and N) in the complexes, and the experimental value on the verge of the theoretical value, indicating that the complexes obtained in the experiment were relatively pure.

Raman and infrared spectroscopy

To determine the complexes structure more accurately, Raman and IR spectra of ligands and complexes were

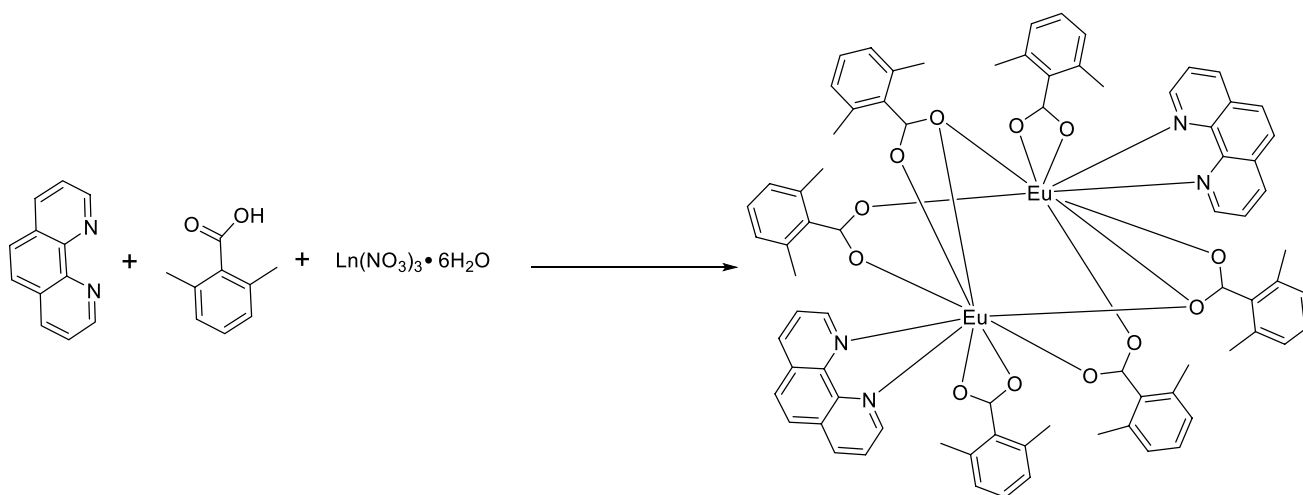
Table 1 Elemental analysis data of complexes 1–3

Complexes	C/(Found)	H/(Found)	N/(Found)
1	60.03(60.41)	4.49(4.66)	3.59(3.51)
2	58.61(58.68)	4.38(4.40)	3.51(3.56)
3	57.84(57.50)	4.36(4.38)	3.46(3.47)

determined. Figure 1 shows the R and IR spectra of acid ligand, neutral ligand, and complexes. The spectral data were shown in Table 2. As you can see from the picture that the characteristic absorption peak of carboxylic group $\nu_{C=O}$ in acidic ligand appears at 1639 cm⁻¹(R), 1690 cm⁻¹(IR), however, this peak does not appear in the complexes. The characteristic absorption peaks of $\nu_{as(COO^-)}$ and $\nu_{s(COO^-)}$ appear in the complexes, they belong to carboxylic acid anions, located at 1587–1602 cm⁻¹(R), 1615–1618 cm⁻¹(IR) and 1444–1451 cm⁻¹(R), 1451–1457 cm⁻¹(IR) respectively. By comparing the neutral ligand with the complexes, the characteristic peaks of phen $\nu_{C=N}$ (1564 cm⁻¹) (R), (1602 cm⁻¹) (IR) have an obvious shift. Indicating that the N atoms of phen ligand were coordinated with lanthanide complexes (Yao et al. 2006). The characteristic absorption peaks of Ln–O and Ln–N were discovered at 405–407 cm⁻¹(IR), 416–418 cm⁻¹(R), and 272–279 cm⁻¹(IR), respectively. It shows that the oxygen atoms in 2,6-DMBA and the nitrogen atoms in phen coordinate with the central metal ion (He et al. 2014; Wang et al 2016).

Description of crystal structure

The three complexes were divided into two types by single-crystal X-ray diffraction, the first type was complex 1, and the second type were complexes 2 and 3. Complexes



Scheme 1 Synthesis scheme of complex 1

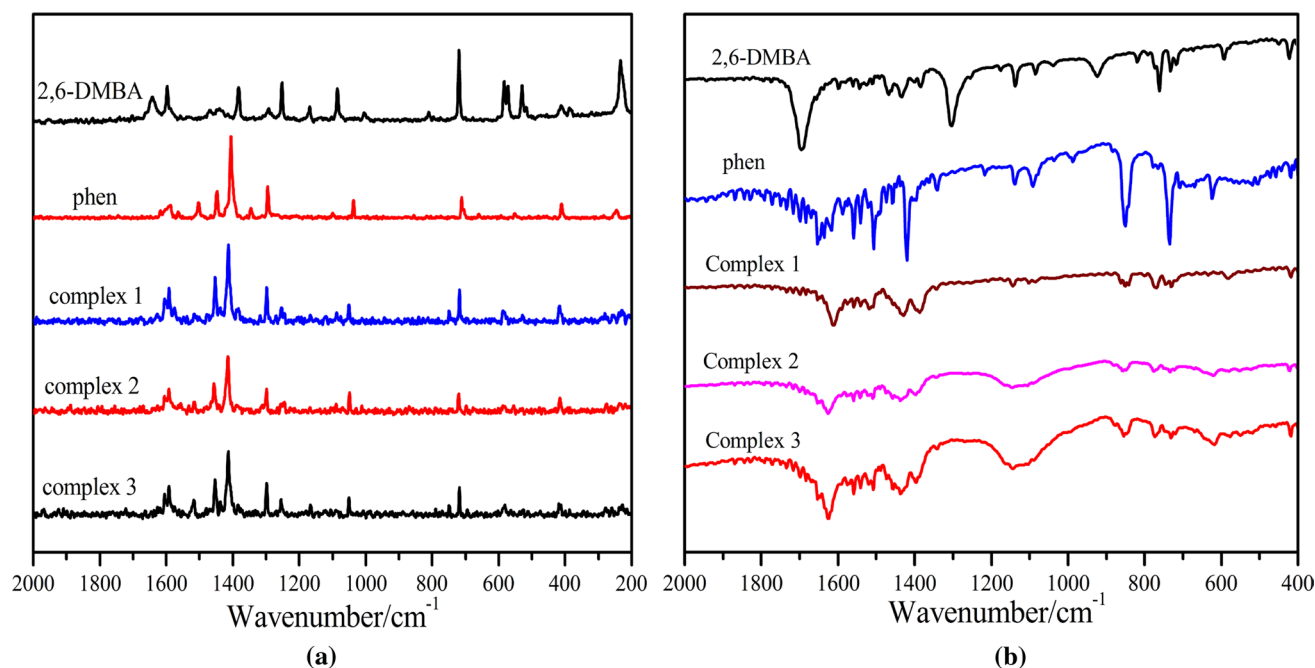


Fig. 1 R **a** and IR **b** Spectra of ligands and complexes

Table 2 Characteristic bands(cm^{-1}) of Raman and infrared spectra of ligands and the title complexes

Ligands/complexes	$\nu_{\text{C=N}}$		$\delta_{\text{C-H}}$		R	$\nu_{\text{C=O}}$		$\nu_{\text{as(COO⁻)}}$		$\nu_{\text{s(COO⁻)}}$		$\nu_{\text{(Ln-O)}}$		$\nu_{\text{(Ln-N)}}$
	IR	R	IR	R		IR	R	IR	R	IR	R	IR	R	R
2,6-DMHBA						1690	1639							
phen	1602	1564	909	806	707									
1	1582	1583	855	772	732			1615	1587	1451	1449	416	405	278
2	1582	1583	856	773	732			1618	1588	1457	1450	418	405	279
3	1582	1585	855	771	735			1615	1591	1457	1452	416	407	278

2 and 3 contain disordered solvent molecules removed by the SQUEEZE procedure. These disordered solvent molecules can be calculated by the number of electrons contained in the structural units combined with elemental analysis and thermogravimetric analysis (Boutar et al. 2019). Among them, the structural units of complexes 2 and 3 contain $18.5 e^-$ and $36.9 e^-$, respectively. The results show that complexes 2 and 3 contain 1.5 and 2.5 disordered water molecules, respectively. Table 3 shows the crystallographic structure data and refined crystal structure parameters of complexes 1–3. The lengths of selected hydrogen bonds were listed in Table 4. Next, we take complexes 1 and 3 as examples to introduce the crystal structure of the complexes. Table 5 lists the hydrogen bond parameters of the three complexes.

[Eu(2,6-DMBA)₃(phen)]₂(1)

As shown in Fig. 2a, complex 1 has a unique binuclear structure and belongs to the triclinic system with space group $P\bar{1}$. It was made up of two Eu(III) ion, six 2,6-DMBA and two phen, and the coordination number was nine. The seven oxygen atoms O5 and O6, O3 and O4, O1, O2 and O1' in 2,6-DMBA were coordinated by chelating bidentate, bridged bidentate and bridged tridentate, respectively. The two N atoms in the phen ligand were coordinated by bidentate chelation. The coordination environment of the complex was a distorted single cap tetragonal antiprism (Fig. 2b). The coordination mode of 2, 6-dimethylbenzoic acid was shown in Fig. 3. Comparative the bond lengths of the central atom of the complex with O and N in Table 4, the

Table 3 X-ray diffraction data and refinement details of complexes 1, 2 and 3

Complexes	1	2	3
Empirical formula	C ₇₈ H ₇₀ Eu ₂ N ₄ O ₁₂	C ₇₈ H ₇₃ Gd ₂ N ₄ O _{13.5}	C ₇₈ H ₇₅ Tb ₂ N ₄ O _{14.5}
Formula weight	1559.32	1596.93	1614.95
Temperature/K	293(2)	293(2)	293(2)
Wavelength/ Å	0.71073	0.71073	0.71073
Crystal system	Triclinic	Triclinic	Triclinic
Space group	<i>P</i> 1	<i>P</i> 1	<i>P</i> 1
<i>a</i> /Å	12.3564(11)	12.0512(13)	12.0267(13)
<i>b</i> /Å	12.7716(12)	12.8118(15)	12.7645(15)
<i>c</i> /Å	12.9532(12)	13.8887(15)	13.8560(15)
<i>α</i> /°	114.266(5)	65.060(1)	65.634(1)
<i>β</i> /°	103.978(3)	74.023(2)	74.915(2)
<i>γ</i> /°	103.277(2)	76.661(2)	76.989(2)
Volume/Å ³	1678.7(3)	1853.1(4)	1854.0(3)
Z, Calculated density/mg.m ⁻³	6, 1.542	1, 1.407	1, 1.409
Absorption coefficient/mm ⁻¹	1.919	1.835	1.953
<i>F</i> ₍₀₀₀₎	788	790	792
Crystal size/mm	0.25 × 0.09 × 0.04	0.16 × 0.08 × 0.03	0.27 × 0.11 × 0.06
Theta range for data collection /°	1.89–25.02	2.17–25.02	2.18–25.02
Limiting indices	– 7 ≤ <i>h</i> ≤ 14 – 14 ≤ <i>k</i> ≤ 15 – 15 ≤ <i>l</i> ≤ 15	– 14 ≤ <i>h</i> ≤ 14 – 14 ≤ <i>k</i> ≤ 15 – 12 ≤ <i>l</i> ≤ 16	– 11 ≤ <i>h</i> ≤ 14 – 15 ≤ <i>k</i> ≤ 14 – 16 ≤ <i>l</i> ≤ 16
Reflections collected/unique	8218/5828 [<i>R</i> _(int) = 0.1069]	9544/6440 [<i>R</i> _(int) = 0.1435]	9536/6456 [<i>R</i> _(int) = 0.0767]
Completeness to theta = 25.02°	98.0%	98.3%	98.6%
Max. and min. transmission	0.9272 and 0.6455	0.9268 and 0.5514	0.8918 and 0.6206
Data/restraints/parameters	5828/0/439	6440/570/433	6456/0/439
Goodness-of-fit on <i>F</i> ²	1.070	1.092	1.078
Final <i>R</i> indices [<i>I</i> > 2σ(<i>I</i>)]	<i>R</i> ₁ = 0.1018 w <i>R</i> ₂ = 0.2474	<i>R</i> ₁ = 0.1301 w <i>R</i> ₂ = 0.3069	<i>R</i> ₁ = 0.0742 w <i>R</i> ₂ = 0.1778
<i>R</i> indices (all data)	<i>R</i> ₁ = 0.1241 w <i>R</i> ₂ = 0.2710	<i>R</i> ₁ = 0.1937 w <i>R</i> ₂ = 0.3303	<i>R</i> ₁ = 0.0915 w <i>R</i> ₂ = 0.1874
Largest diff. peak and hole (e Å ⁻³)	4.432 and -1.932	2.834 and -2.034	1.946 and -3.459

Table 4 Bond lengths for complexes 1–3

Complex 1	Bond length/(Å)	Complex 2	Bond length/(Å)	Complex 3	Bond length/(Å)
Eu(1)-O(3)	2.331(8)	Gd(1)-O(1)#1	2.291(12)	Tb(1)-O(2)#1	2.303(6)
Eu(1)-O(1)#1	2.354(9)	Gd(1)-O(4)#1	2.341(12)	Tb(1)-O(3)	2.303(6)
Eu(1)-O(4)#1	2.435(8)	Gd(1)-O(3)	2.360(11)	Tb(1)-O(5)	2.344(6)
Eu(1)-O(5)	2.443(9)	Gd(1)-O(6)	2.389(11)	Tb(1)-O(4)#1	2.362(6)
Eu(1)-O(6)	2.453(9)	Gd(1)-O(2)	2.532(12)	Tb(1)-O(1)	2.493(7)
Eu(1)-O(2)	2.554(9)	Gd(1)-O(5)	2.569(13)	Tb(1)-O(6)	2.530(7)
Eu(1)-N(1)	2.618(9)	Gd(1)-N(2)	2.608(17)	Tb(1)-N(2)	2.582(8)
Eu(1)-O(1)	2.644(9)	Gd(1)-N(1)	2.637(14)	Tb(1)-O(2)	2.618(6)
Eu(1)-N(2)	2.716(11)	Gd(1)-O(1)	2.642(12)	Tb(1)-N(1)	2.640(7)

bond lengths of Eu-N and Eu-O were (2.618–2.716 Å) and (2.331–2.644 Å), respectively. It can be concluded that the average bond length of Eu and O was smaller than that of Eu and N. This was also why neutral ligands were lost before

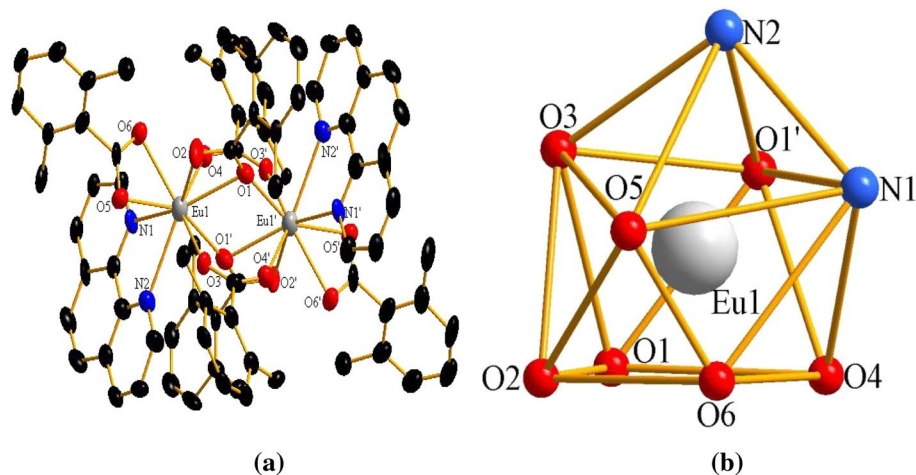
acidic ones during thermal decomposition. The adjacent structural units form a 1D chain structure along the *c* direction through the interaction of hydrogen bonds (3.385 Å). The 1D supramolecular structure in the *c*-direction forms a

Table 5 Selected Hydrogen-Bond Lengths (Å) and Angles (°) complexes 1–3

Complexes	D-H	H...A	D...A	D-H...A
<i>1</i>				
C9-H9B...O4	0.96	2.60	3.5254(3)	163
C18-H18B...O4	0.96	2.49	3.8294(3)	100
C27-H27B...O5	0.96	2.48	3.1484(3)	127
C37-H37...O3	0.93	2.31	2.9447(3)	125
<i>2</i>				
C17-H17A...O3	0.96	2.03	2.7814(3)	134
C18-H18C...O4	0.96	2.18	2.6405(3)	108
C26-H26A...O5	0.96	2.17	2.9033(3)	132
C27-H27C...O6	0.96	2.40	2.9293(3)	115
C28-H28...O4	0.93	2.25	2.9020(3)	126
C30-H30...O6	0.93	2.58	3.3842(4)	144
C37-H37...O3	0.93	2.39	3.0125(4)	124
<i>3</i>				
C17-H17A...O3	0.96	2.38	2.7455(3)	102
C18-H18B...O4	0.96	2.44	2.7720(3)	100
C28-H28...O3	0.93	2.27	2.9051(3)	125
C30-H30...O5	0.93	2.60	3.3863(4)	143
C37-H37...O4	0.93	2.43	2.9970(3)	120

2D supramolecular structure in the *b*-axis and *c*-axis through hydrogen bonding between ligands (Figs. 4a, b).

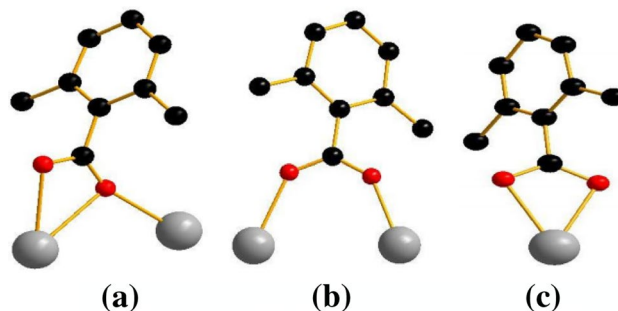
It was different from the complex $[\text{Eu}(\text{2,6-DMBA})_3(\text{5,5'-DM-2,2'-bipy})_2]$ (2,6-DMBA = 2,6-dimethylbenzoic acid, 5,5'-DM-2,2'-bipy = 5,5'-dimethyl-2,2'-bipyridine) reported by Li Yingying (Li et al. 2019). It has been reported that the complex was centered on a 9-coordinated Eu(III) ion and forms a twisted tetragonal inverse prism geometry with surrounding nitrogen and oxygen atoms. The difference was that the reported complexes crystallize in the $P2_1/c$ -space group of the monoclinic system. The two complexes have the same central ion and acid ligand, but the difference was

Fig. 2 a The crystal structure of 1. b The polyhedral model of Eu^{3+} ion center

that there were two benzene rings in 5,5'-DM-2,2'-bipy and three benzene rings in phen. The steric hindrance of the complexes results in different spatial crystal systems.

$[\text{Tb}(\text{2,6-DMBA})_3(\text{phen})_2 \cdot 2.5\text{H}_2\text{O}(\mathbf{3})]$

It was centered on a 9-coordinated Tb(III) ion and coordinates with seven oxygen atoms in the 2, 6-DMBA ligand and two nitrogen atoms in the phen ligand (Fig. 5a). Oxygen and nitrogen atoms coordinate with Tb(III) ion by chelating bidentate, bridged bidentate, and bridged tridentate respectively. The coordination environment of complex 3 was a distorted mono-capped square anti-prismatic (Fig. 5b). The average bond length of Tb-N(2.611 Å) was greater than that of Tb-O(2.421 Å), this data can be obtained from Table 4. This further shows that the coordination ability of nitrogen atom with lanthanide ion was not as good as that of oxygen atom with lanthanide ion compared with complex 1, the average bond length of Eu-N(O) was slightly longer than that of Tb-O(N), which was due to the "lanthanide contraction" (Deng et al. 2010). Adjacent structural units form 1D chains along the *c*-axis through weak hydrogen bond interactions (3.385 Å) between oxygen atoms in the acid ligand and carbon atoms in the neutral ligand (Fig. 6).

**Fig. 3** Coordination mode of 2, 6-DMBA⁻

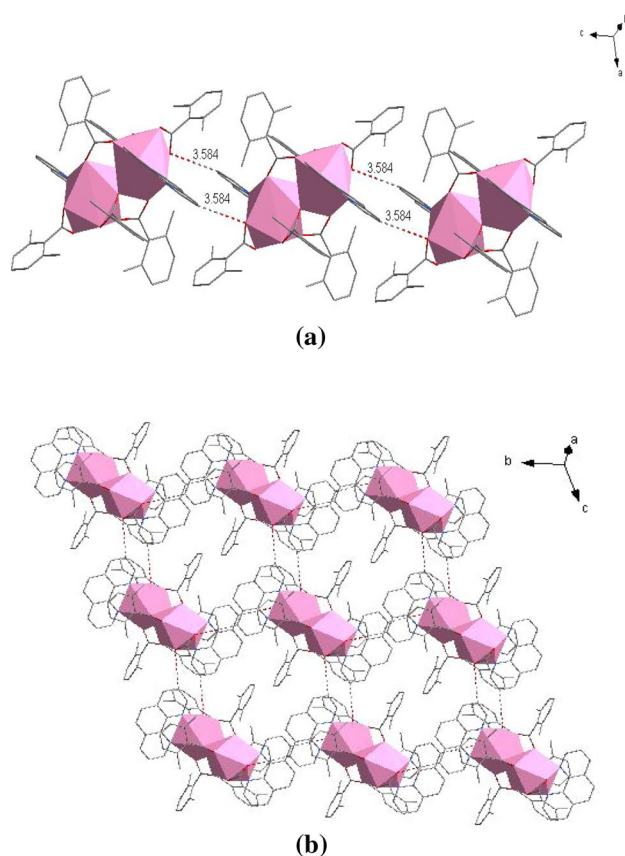


Fig. 4 **a** The one-dimensional chains structure along the *c* axis. **b** The two-dimensional sheet is about the *bc* plane

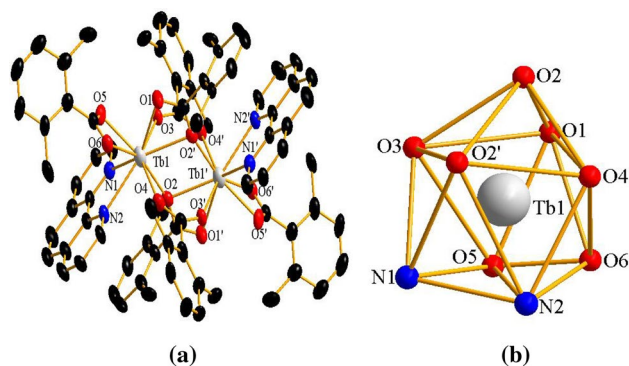


Fig. 5 **a** The crystal structure of 3. **b** The polyhedral model of Tb^{3+} ion center

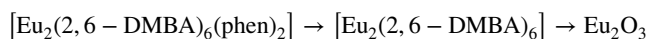
The complex $[Tb_2L_6(phen)_2]$ ($L = 4$ -fluorophenylseleuoacetic acid, phen = 1,10-phenanthroline) was reported by Zhang Fan (Zhang et al. 2021). It has many similarities with the complex 3 synthesized in this paper. For example, it has the same coordination number, coordination environment, and coordination mode. The different was that the space group of the reported complexes was $P2_1/c$. In addition,

the complex 3 synthesized in this paper contains disordered solvent water molecules. This may be due to the different number of substituents in acidic ligands, resulting in different steric hindrance, resulting in different spatial crystal systems of complexes.

Thermal analysis

The thermal behavior of the complexes with temperature was studied. Table 6 lists the thermal decomposition data obtained by simulating the air atmosphere, and the heating rate was $10\text{ K}\cdot\text{min}^{-1}$. Figure 7 was the TG-DTG-DSC curves of complexes 1–3. Complexes 2 and 3 have the same crystal structure, so their thermal decomposition process was similar. Therefore, the thermal behavior of complexes 1 and 3 were described in detail.

Combined with TG and DTG analysis (Fig. 7a), complex 1 was decomposed in two steps. At 502.15 K, the decomposition of the first step begins, and the weight loss rate was 23.17%, which was close to the calculated value of losing two phen (calcd: 23.11%). This suggests that the breakdown of the first step can be attributed to the loss of phen ligands. The weight loss of the second step started at 626.15 K and ended at 974.15 K, with a weight loss rate of 53.60% (calcd: 54.32%), indicating that the decomposition of the second step could be attributed to the decomposition of six acid ligands. The total weight loss rate was 76.77%, which was in good agreement with the theoretical value (77.43%). The final product was Eu_2O_3 . In conclusion, the Eu–N bond was destroyed prior to the Eu–O bond. The thermal decomposition process of the complex 1 was as follows:



DTG curve showed that complex 3 was decomposed in three steps (Fig. 7c). In the temperature range of 395.15 ~ 502.15 K, the first step weight loss rate was 2.70% (calcd: 2.78%). This step of decomposition can be attributed to the loss of 2.5 water molecules. Unlike complex 3, complex 2 loses 1.5 disordered water molecules in the first step. The second step of weightlessness occurs at 502.15 ~ 608.15 K, and the weightlessness rate was 22.82% (calcd: 22.27%). Thus, the second step of decomposition can be attributed to the loss of two neutral ligands. The last step of decomposition occurs between 608.15–938.15 K, and the weight loss rate was right around the theoretical value of 51.85% (found: 52.58%) of the loss of six acidic ligands. Combined with the above analysis, the final remaining product was 21.9% (calcd 23.1%), and the final product was Tb_4O_7 (Łyszczek et al. 2016; Wang et al. 2011). The thermal decomposition process of the complex 3 was as follows:

Fig. 6 The one-dimensional chains structure along the *b* axis

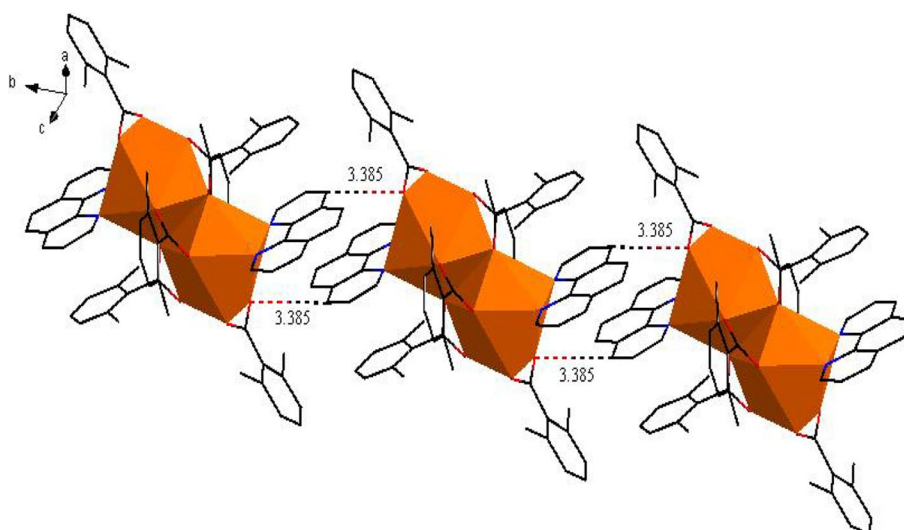
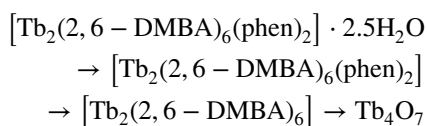


Table 6 Thermal analysis data of complexes 1–3 in simulated air atmosphere

Complex	Steps	Temperature range/K	DTG T_p /K	Mass loss rate/%		Probable expelled groups	Residue
				Found	Calcd		
1	I	502.15–626.15	560.85	23.17	23.11	2(phen)	[Eu ₂ (2,6-DMBA) ₆]
	II	626.15–974.15	706.75	53.60	54.32	6(2,6-DMBA)	Eu ₂ O ₃
				76.77	77.43		
2	I	402.15–509.15	434.05	1.55	1.69	1.5(H ₂ O)	[Gd ₂ (2,6-DMBA) ₆ (phen) ₂]
	II	509.15–602.15	555.65	22.95	22.57	2(phen)	[Gd ₂ (2,6-DMBA) ₆]
	III	602.15–930.15	750.65	53.76	53.95	6(2,6-DMBA)	Gd ₂ O ₃
				78.26	78.21		
3	I	395.15–502.15	433.45	2.70	2.78	2.5(H ₂ O)	[Tb ₂ (2,6-DMBA) ₆ (phen) ₂]
	II	502.15–608.15	554.55	22.82	22.27	2(phen)	[Tb ₂ (2,6-DMBA) ₆]
	III	608.15–938.15	752.05	52.58	51.85	6(2,6-DMBA)	Tb ₄ O ₇
				78.1	76.9		



Evolved gas study during thermal decomposition

In order to further determine the thermal decomposition products, the three-dimensional infrared stacking diagram of the complexes in the thermal decomposition process was determined.

Figures 8a–c shows the three-dimensional infrared stacking diagram of the gas escaping from complexes 1–3 during thermal decomposition. No signal peak at the first stage was observed from the three-dimensional infrared stacking diagram of complexes 2–3, which may be due to less gas generation and a longer instrument pipeline. Therefore, complexes

1–3 have similar three-dimensional infrared stacking patterns. We take complex 3 as an example.

The two-dimensional infrared spectra at 489.32 K and 753.02 K were obtained from the three-dimensional infrared stacking diagram (Fig. 9c). The characteristic absorption bands of CO₂ (2318–2367, 683 cm⁻¹) and H₂O (3563–3847 cm⁻¹) were observed in the two-dimensional spectrum at a temperature of 489.32 K. Meanwhile, the absorption bands of organic molecular fragments were also detected: $\nu_{\text{C-H}}$ (3083–3401 cm⁻¹), $\nu_{\text{C=C}}$ (1569 cm⁻¹), $\nu_{\text{C=N}}$ (1589 cm⁻¹), $\nu_{\text{C-N}}$ (1191 cm⁻¹) and $\gamma_{\text{C-H}}$ (764, 865, 1062 cm⁻¹). It indicates that the phen ligand was decomposed in this process. The characteristic absorption bands of CO₂ (2163–2291 cm⁻¹, 668 cm⁻¹) and H₂O (3566–3776 cm⁻¹) can be observed from the two-dimensional spectra at 753.02 K. It indicates that the remaining acidic ligands escape as gaseous CO₂ and H₂O in this step.

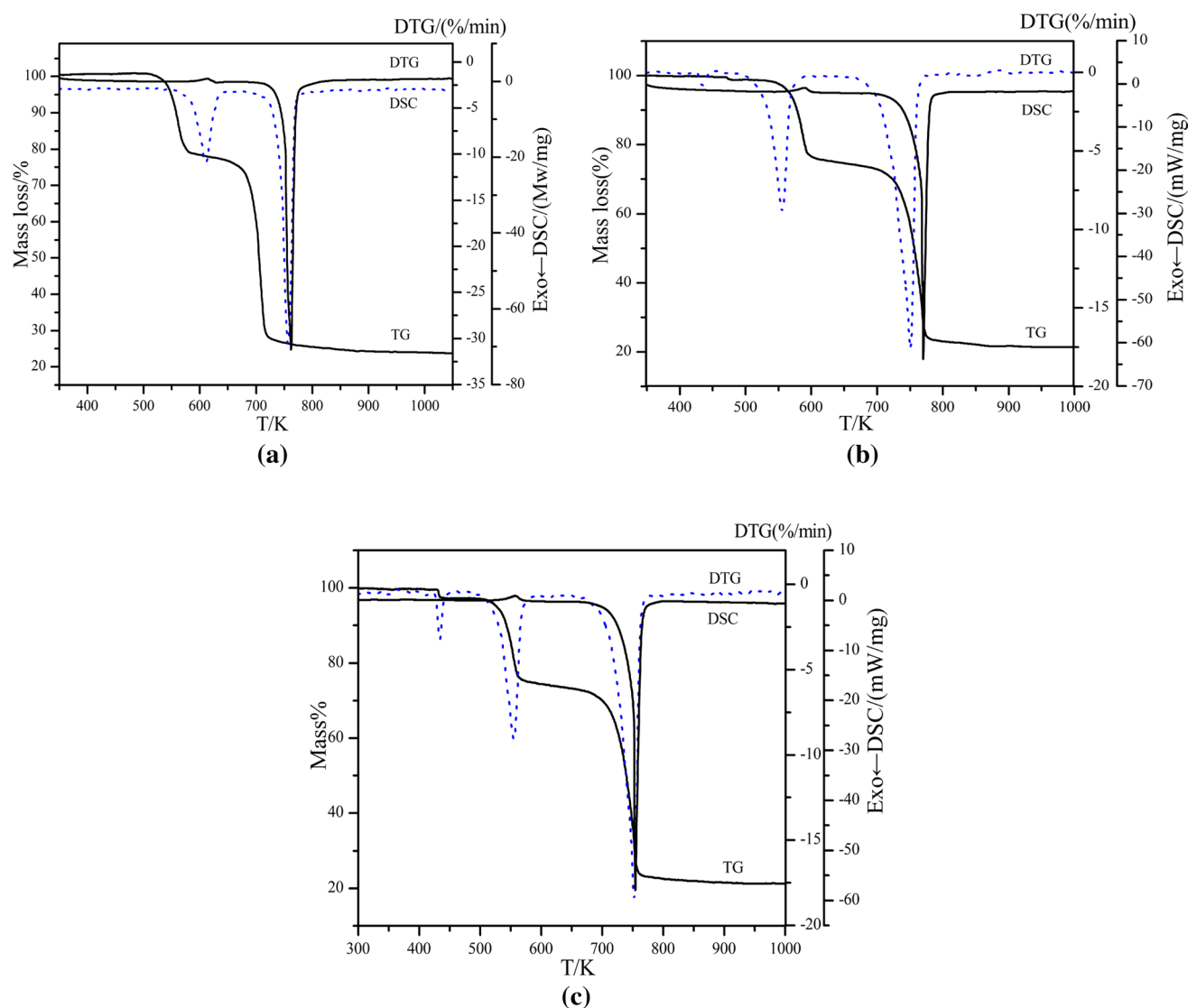


Fig. 7 TG-DTG-DSC curves of the complex 1 (a); complex 2 (b); complex 3 (c)

This was in compliance with the thermal decomposition process of the above complexes.

Luminescent property

To further probe the luminescent property of lanthanide complexes, the solid-state fluorescence spectra of complexes 1 and 3 were determined by fluorescence spectrometer. Complexes 1 and 3 emit intense red and green light respectively under UV lamp irradiation (Figs. 10, 11). The excitation spectra of complex 1 was shown in Fig. 10a. The $\pi \rightarrow \pi^*$ electron transition of organic ligand makes complex 1 has a wide absorption band in the range of 250–450 nm, this further suggests that organic ligands can act as antennas

to efficiently transfer absorbed energy to Eu(III) ions. However, due to the f-f configuration transition of Eu(III) ions, other weak excitation peaks appear in this wavelength range. The emission spectrum (Fig. 10b) was measured within the limits of 500–750 nm with 335 nm as the excitation wavelength. The intensity of ${}^5D_0 \rightarrow {}^7F_2$ (620 nm) transition was higher than that of ${}^5D_0 \rightarrow {}^7F_0$ (579 nm), ${}^5D_0 \rightarrow {}^7F_1$ (590 nm), ${}^5D_0 \rightarrow {}^7F_3$ (650 nm) and ${}^5D_0 \rightarrow {}^7F_4$ (695 nm). This was also the reason why Eu complexes emit red light (Ridenour et al. 2017).

In the range of 250–450 nm, an obvious broadband absorption was observed in the excitation spectrum of complex 3 (Fig. 11a), this was mainly due to the $\pi \rightarrow \pi^*$ electron transition of organic (Rybak et al. 2012). The emission

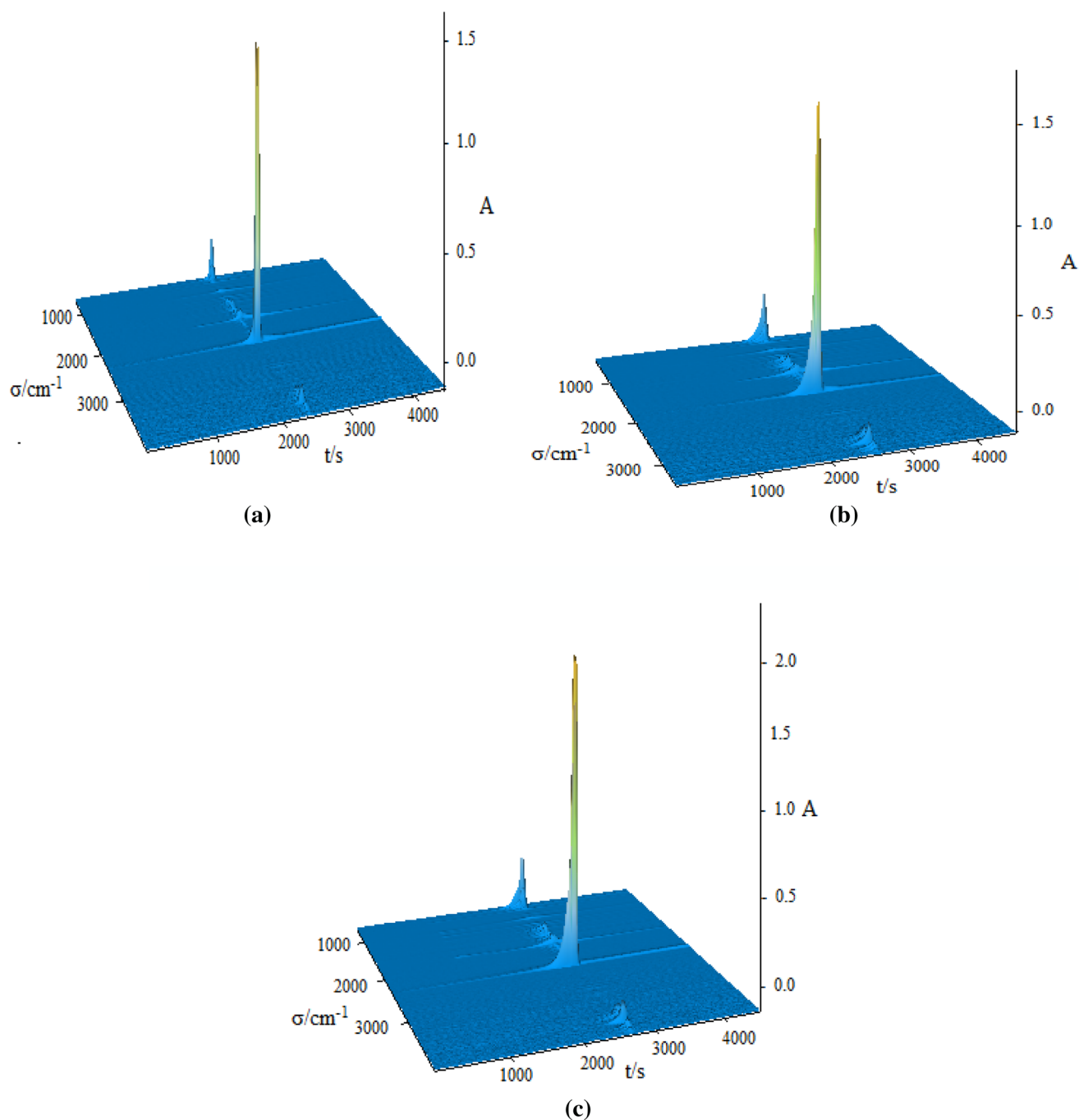


Fig. 8 The 3D infrared spectrum stacking diagram of gas escaping from complex 1 (a); complex 2 (b); complex 3 (c)

spectrum of Fig. 11b was measured at 345 nm, and four characteristic transitions of Tb(III) ion can be observed within the limits of 500–750 nm. The transition intensity of ${}^5D_4 \rightarrow {}^7F_5$ at 545 nm was larger than that of ${}^5D_4 \rightarrow {}^7F_6$ (490 nm), ${}^5D_4 \rightarrow {}^7F_4$ (590 nm) and ${}^5D_4 \rightarrow {}^7F_3$ (620 nm). It was also the reason why complex 3 emits strong green light

under ultraviolet light (Łyszczek et al. 2015). It has the same characteristic transition and luminescence color as the Tb complex published by Ye et al. (2010).

The emission spectra of complexes 1 and 3 were brought into the color coordinate diagram, respectively. The

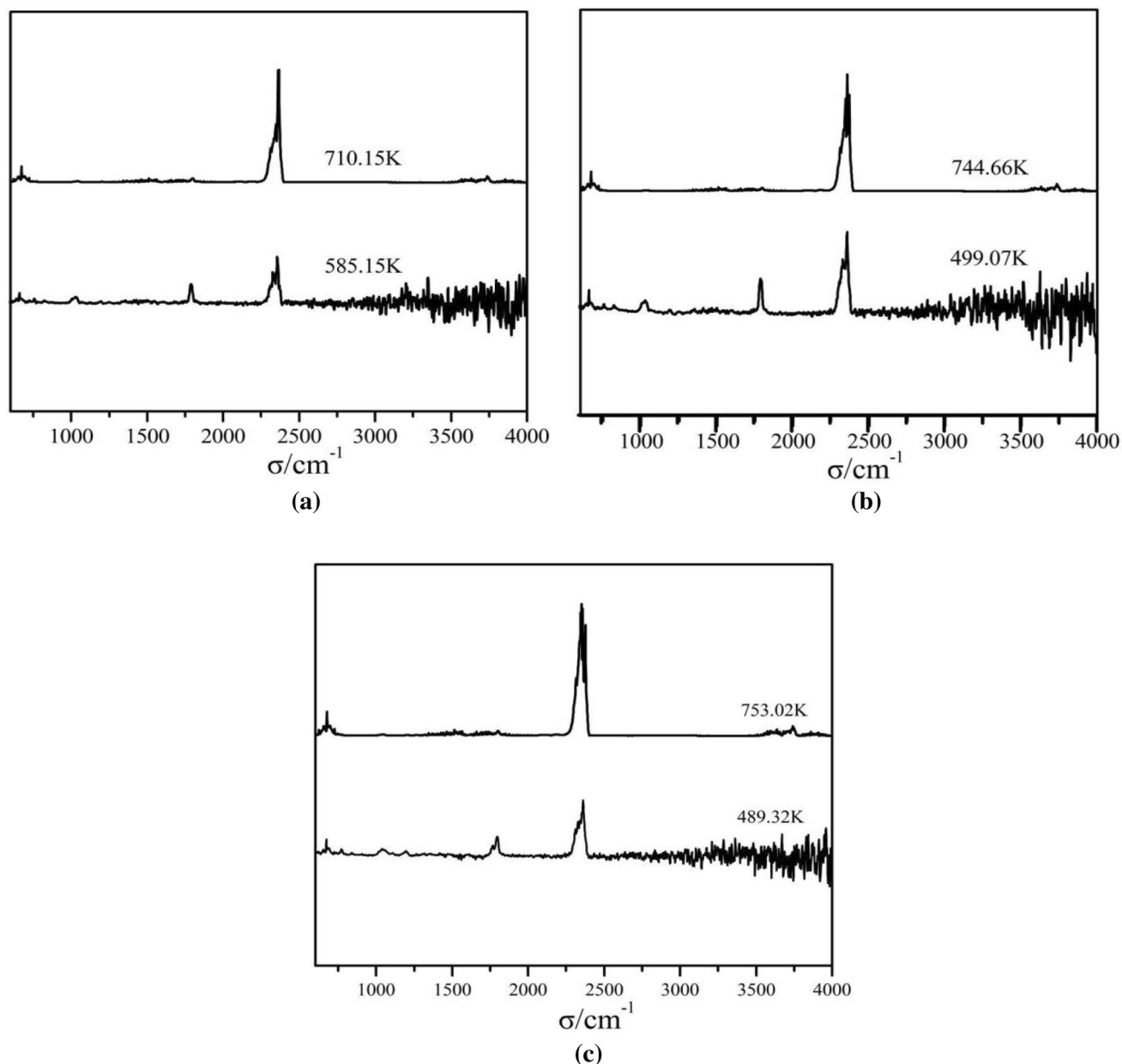


Fig. 9 The 2D infrared spectra of complex 1 (a); complex 2 (b); complex 3 (c)

calculated color coordinates were (0.6633, 0.3354), (0.3425, 0.5968). Complexes 1 and 3 were located in the red and green regions, respectively (Fig. 12).

In addition, the fluorescence lifetime of lanthanide complexes were also of great meaning in the study of physical, chemical, and biological excitation kinetics. The fluorescence lifetime decay curves of solid complexes 1 and 3 at the optimal excitation and emission wavelengths were

measured (Figs. 13, 14). The fluorescence lifetime data of the complexes were fitted by double exponential function equation: $I(t) = B_1 \cdot \exp(-t/\tau_1) + B_2 \cdot \exp(-t/\tau_2)$, and the corresponding fitting parameters B_1 , B_2 , and decay time were obtained τ_1 , τ_2 . At the same time, the fluorescence lifetimes of complexes 1 and 3 were calculated by formula $\tau = (B_1\tau_1^2 + B_2\tau_2^2) / (B_1\tau_1 + B_2\tau_2)$ as 1.034 ms and 0.557 ms, respectively.

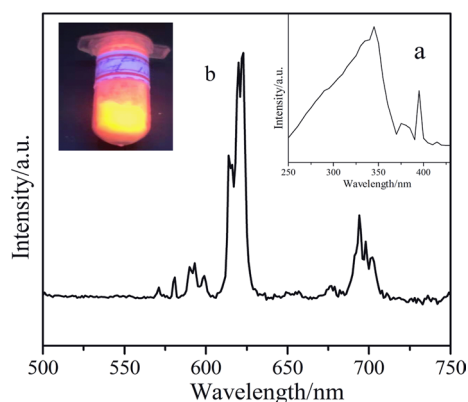


Fig. 10 The solid-state excitation (a) and emission (b) spectra for 1

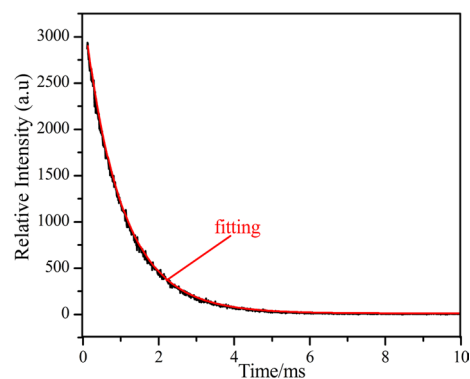


Fig. 13 Fluorescence attenuation and fitting curve of 1

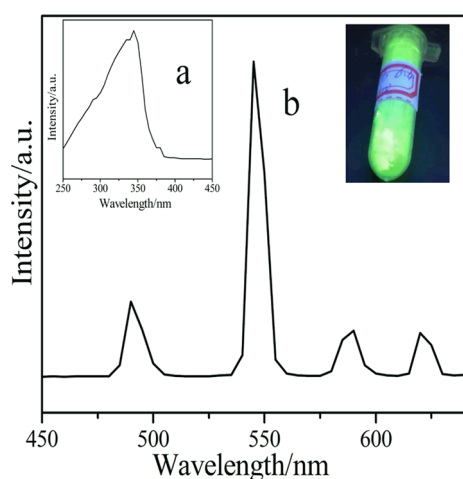


Fig. 11 The solid-state excitation (a) and emission (b) spectra for 3

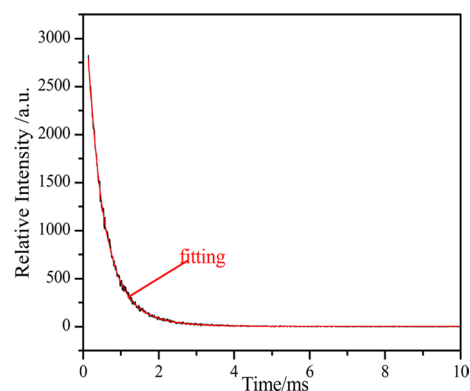


Fig. 14 Fluorescence attenuation and fitting curve of 3

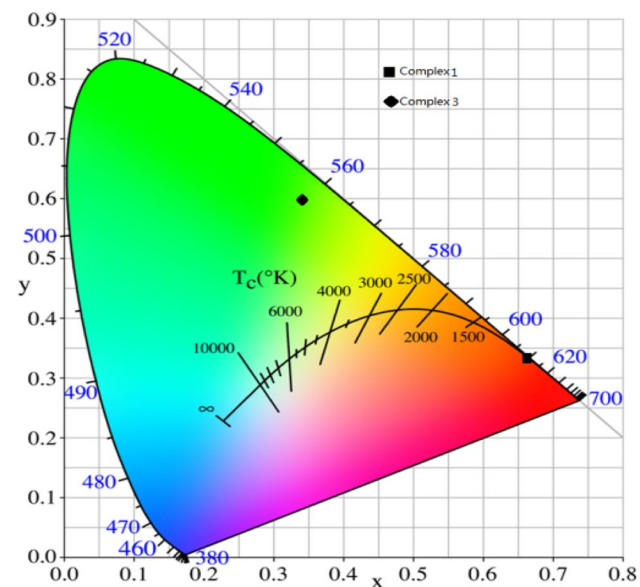


Fig. 12 CIE chromaticity diagram of 1 and 3 corresponding to fluorescence emission spectrum

In summary, complexes 1 and 3 can emit characteristic transitions corresponding to lanthanide ions and have strong fluorescence intensity and long lifetime. Therefore, these two complexes have potential application prospects in the field of luminescent materials.

Conclusions

In this paper, three lanthanide complexes with novel structures were prepared and characterized by conventional solution method using 2, 6-DMBA, and phen as the ligands. The results show that the complexes 1–3 were all binuclear complexes with 9 coordination and all crystallize in the $P\bar{1}$ -space group of triclinic crystal system. The different supramolecular structures of complexes 1 and 2–3 may be caused by different hydrogen bond interactions and lanthanide contraction effects. However, the binuclear units of complexes 1–3 form 1D chain structure through hydrogen bond interaction. TG-DSC/FTIR study showed that the three complexes had good thermal

stability. Solid-state fluorescence test shows that terbium complex and europium complex emit strong characteristic green and red light, respectively. It lays a foundation for the application of lanthanide complexes in the field of luminescent materials.

Supplementary Information The online version contains supplementary material available at <https://doi.org/10.1007/s11696-022-02211-2>.

Acknowledgements The research work was supported by the National Natural Science Foundation of China (No. 21473049).

Author's contributions XW performed the experiments and wrote the paper. LG and JZ collected the data and statistically analyzed the data. NR and YM designed the research and wrote the paper. All authors read and approved the final manuscript. XW, NR, YM, LG, and JZ contributed equally to this work.

References

- Ahmed Z, Iftikhar K (2010) Synthesis and visible light luminescence of mononuclear nine-coordinate lanthanide complexes with 2,4,6-tris(2-pyridyl)-1,3,5-triazine. *Inorg Chem Commun* 13:1253–1258. <https://doi.org/10.1016/j.inoche.2010.07.009>
- Bai FF, Yao BL, Wang RR, Wang W, Wang QL, Ma Y, Li LC (2021) Structures and magnetic properties of five lanthanide-radical complexes constructed by 8-methoxyquinoline substituted tridentate chelating nitronyl nitroxide radical. *J Solid State Chem* 298:122115. <https://doi.org/10.1016/j.jssc.2021.122115>
- Boutar M, Desroches CN, Habib Noamane M, Bois L, Gautier-Luneau I, Abidi R, Luneau D (2019) Coordination polymers of zinc(II) and manganese(II) made by complexation of calix[4] arene functionalized with carboxylates afford alveolar materials. *Inorg Chim Acta* 486:562–567. <https://doi.org/10.1016/j.ica.2018.11.001>
- Chesnokov GA, Topchiy MA, Asachenko AF, Muravyev NV, Grishin NV, Nikiforova AS, Utochnikova VV, Khrustalev RVB, Nechaev NV (2018) Rare-Earth Complexes with the 5,5'-bitetrazolate ligand-synthesis, structure, luminescence properties, and combustion catalysis. *Eur J Inorg Chem* 2018:805–815. <https://doi.org/10.1002/ejic.201701154>
- Deng ZP, Kang W, Huo LH, Zhao H, Gao S (2010) Rare-earth organic frameworks involving three types of architecture tuned by the lanthanide contraction effect: hydrothermal syntheses, structures and luminescence. *Dalton Trans* 39:6276–6284. <https://doi.org/10.1039/c0dt00031k>
- Di YQ, Cui XW, Liu YL, Zhou CS, Ren YL, Di YY, Yang X (2019) Crystal structure, optical properties, and antibacterial activity of rare earth complexes with designed 2-carbonyl propionic acid-4-nitrobenzoyl hydrazone. *Polyhedron* 171:571–577. <https://doi.org/10.1016/j.poly.2019.07.036>
- Dobies Navia MV, Alves Galico D, Junior Caires F, Luiz M, Spezia Nunes JR (2018) Synthesis, thermal behavior, and spectroscopic study of the solid nalidixate of selected light trivalent lanthanides. *J Therm Anal Calorim* 132:1717–1727. <https://doi.org/10.1007/s10973-018-7042-0>
- Du DD, Ren N, Zhang JJ (2021) A series of lanthanide complexes with 2-fluorobenzoic acid and 5,5'-dimethyl-2,2'-bipyridine: synthesis, supramolecular structures, spectroscopy and thermal behaviour. *J Solid State Chem* 300:122198. <https://doi.org/10.1016/j.jssc.2021.122198>
- Guo X, Sun J, Li X, Yin YT, Zhou C, Su ZM, Khakhinov V (2021) Temperature sensitive properties and preparation of europium complexes with double ligands. *Luminescence*. 36:1476
- He SM, Sun SJ, Zheng JR, Zhang JJ (2014) Molecular spectrum of lanthanide complexes with 2,3-dichlorobenzoic acid and 2,2'-bipyridine. *Spectrochim Acta, Part A* 123:211–215. <https://doi.org/10.1016/j.saa.2013.12.023>
- Ji QS, Wen WF, Liu SZ, Liu X, He LF, Yi XG, Chen WT (2021) Series of novel lanthanide complexes with a ladder-shaped 1-D double chain: preparation, structures and photophysical properties. *Inorg Chim Acta* 519:120278. <https://doi.org/10.1016/j.ica.2021.120278>
- Kariaka NS, Trush VA, Gawryszewska P, Dyakonenko VV, Shishkina SV, Sliva TY, Vamirkhanov M (2016) Spectroscopy and structure of [LnL3bipy] and [LnL3phen] complexes with CAPH type ligand dimethylbenzoylamidophosphate. *J Lumin* 178:392–399. <https://doi.org/10.1016/j.jlumin.2016.06.018>
- Kong K, Zhang HX, Ma RJ, Chen YN, Chu HB, Zhao YL (2013) Synthesis, characterization and enhanced luminescence of terbium complexes with 2-pyrazinecarboxylic acid and butanedioic acid by inert-fluorescent lanthanide ions. *J Rare Earths* 31:32–36. [https://doi.org/10.1016/S1002-0721\(12\)60230-0](https://doi.org/10.1016/S1002-0721(12)60230-0)
- Kobyłka KMJ, Lis T, Ślepokura K, Lisowski J (2020) Versatile binding modes of chiral macrocyclic amine towards rare earth ions. *Eur J Inorg Chem* 2020:2096–2104. <https://doi.org/10.1002/ejic.202000247>
- Li YY, Ren N, He SM, Wang SP, Zhang JJ (2019) Construction of lanthanide complexes based on 2,6-dimethylbenzoic acid and 5,5'-dimethyl-2,2'-bipyridine: Supramolecular structures, thermodynamic properties and luminescence. *J Chem Thermodyn* 135:1–8. <https://doi.org/10.1016/j.jct.2019.03.010>
- Łyszczek R, Głuchowska H, Cristovao B, Tarasiuk B (2016) New lanthanide biphenyl-4,4'-diacetates-hydrothermal synthesis, spectroscopic, magnetic and thermal investigations. *Thermochim Acta* 645:16–23. <https://doi.org/10.1016/j.tca.2016.11.001>
- Łyszczek R, Ostasz A, Bartyzel A, Lipke A (2015) Thermal, spectroscopic and luminescence investigations of lanthanide(III) coordination polymers based on V-shaped 4,4'-sulfonyldibenzoic acid. *J Anal Appl Pyrolysis* 115:370–378. <https://doi.org/10.1016/j.jaap.2015.08.018>
- Nascimento ALCS, Ashton GP, Parkes GMB, Ekawa B, Fernandes RP, Carvalho ACS, Ionashiro M, Caires FJ (2019) Novel solid-state compounds of heavy rare-earth (III) picolines. a pyrolytic study using: TG-DSC-IR, HSM-MS and GC-MS. *J Anal Appl Pyrolysis* 144:104709. <https://doi.org/10.1016/j.jaap.2019.104709>
- Pham YH, Trush VA, Korabik M, Amirkhanov VM, Gawryszewska P (2021) Nd³⁺ and Yb³⁺ complexes with N-(diphenylphosphoryl) pyrazine-2-carboxamide as UV-NIR radiation converters and single-ion magnets. *Dyes Pigment* 186:108986. <https://doi.org/10.1016/j.dyepig.2020.108986>
- Qi XX, Shi Q, Ren N, Zhang JJ (2019) A neodymium(III) complex with 3,4,5-triethoxybenzoic acid and 1,10-phenanthroline. *J Therm Anal Calorim* 135:2583–2590. <https://doi.org/10.1007/s10973-018-7269-9>
- Ren N, Wang F, Zhang JJ, Zheng XF (2020) Progress in thermal analysis kinetics. *Acta Phys-Chim Sin* 36:1905062
- Ridenour JA, Carter KP, Butcher RJ, Cahill CL (2017) RE-p-halobenzoic acid-terpyridine complexes, Part II: structural diversity, supramolecular assembly, and luminescence properties in a series of p-bromobenzoic acid rare-earth hybrid materials. *CrystEngComm* 19:1172–1189. <https://doi.org/10.1039/c6ce02355j>
- Rybak JC, Meyer LV, Wagenhofer J, Sextl G, Muller-Buschbaum K (2012) Homoleptic lanthanide 1,2,3-triazolates (infinity)(2–3) [Ln(Tz*)₃] and their diversified photoluminescence properties. *Inorg Chem* 51:13204–13213. <https://doi.org/10.1021/ic301482e>

- Shi XH, Wang WM, Yan LL, Fan CJ, Pang JL, Wu ZL (2021) Crystal structure and single-molecule magnet behavior of a novel tetranuclear Dy(III)-based cluster. *J Mol Struct* 1226:129373. <https://doi.org/10.1016/j.molstruc.2020.129373>
- Sheldrick GM (2015) SHELXT - Integrated space-group and crystal-structure determination. *Acta Crystallogr. Sect a: Found Adv* 71:3–8. <https://doi.org/10.1107/S2053273314026370>
- Sun O, Chen P, Li HF, Gao T, Yan PF (2020) Wheel-like Ln6 luminescent lanthanide complexes covering the visible and near-infrared domains. *CrystEngComm* 22:5200–5206. <https://doi.org/10.1039/d0ce00652a>
- Su SQ, Wang S, Song XZ, Song SY, Qin C, Zhu M, Hao ZM, Zhao SN, Zhang HJ (2012) Syntheses, structures, photoluminescence, and magnetic properties of (3,6)- and 4-connected lanthanide metal-organic frameworks with a semirigid tricarboxylate ligand. *Dalton Trans* 41:4772–4779. <https://doi.org/10.1039/c2dt12346k>
- Wang JJ, Zhang JJ (2020) Thermal analysis kinetics and thermokinetics. *Acta Phys -Chimica Sin* 36(6):1909020. <https://doi.org/10.3866/PKU.WHXB201909020>
- Wang Y, Jin CW, He SM, Ren N, Zhang JJ (2016) Five novel lanthanide complexes with 2-chloroquinoline-4-carboxylic acid and 1,10-phenanthroline: crystal structures, molecular spectra, thermal properties and bacteriostatic activities. *J Mol Struct* 1125:383–390. <https://doi.org/10.1016/j.molstruc.2016.07.007>
- Wang CC, Wang ZH, Gu FB, Guo GS (2011) Three novel lanthanide MOFs constructed from 1,3-benzenedicarboxylic acid and 1,10-phenanthroline: hydrothermal synthesis, crystal structure and thermal properties. *J Mol Struct* 1004:39–44. <https://doi.org/10.1016/j.molstruc.2011.07.014>
- Xiong XJ, Guan L, Wang Y, Liu C, Jin HZ, Chen YX, Wang X (2021) Hydrothermal syntheses, crystal structures and properties of two H₂Tiron-bridged rare earth metal dinuclear complexes with 1,10-phenanthroline ligands. *J Coord Chem* 74:1197–1208. <https://doi.org/10.1080/00958972.2021.1894556>
- Xu XL, Wang Z, Yan CC, Hou XM, Tang SF (2020) Structural variability of rare earth carboxylates based on polydentate carboxylate ligand containing pyridine group. *J Solid State Chem* 292:121708. <https://doi.org/10.1016/j.jssc.2020.121708>
- Yang Y, Chen L, Jiang FL, Yu MX, Wan XY, Zhang B, Hong C (2017) A family of doped lanthanide metal-organic frameworks for wide-range temperature sensing and tunable white light emission. *J Mater Chem C* 5:1981. <https://doi.org/10.1039/c6tc05316e>
- Yao JL, Yuan YX, Gu RN (2006) Raman spectroscopic studies on tropolone complexes with La, Nd, Sm, Yb. *Spectrochim Acta, Part A* 64:1072–1076. <https://doi.org/10.1016/j.saa.2005.09.017>
- Ye HM, Ren N, Zhang JJ, Sun SJ, Wang JF (2010) Crystal structures, luminescent and thermal properties of a new series of lanthanide complexes with 4-ethylbenzoic acid. *New J Chem* 34:533–540
- Zapała L, Woźnicka ME, Byczyński Ł, Zapała W, Kalemekiewicz J (2018) Preparation, spectral properties and thermal decomposition of new ternary complexes of La(III), Ce(III), Pr(III) and Nd(III) ions with N-phenylanthranilic acid and 1,10-phenanthroline. *Thermochim Acta* 659:242–252. <https://doi.org/10.1016/j.tca.2017.12.012>
- Zhang F, Zhang RF, Ru J, Wang J, Li QL, Ma CL (2021) Synthesis, structures, photoluminescence and magnetic properties of three dinuclear lanthanide(III) complexes derived from 4-fluorophenylselenoacetic acid. *Z Anorg Allg Chem* 647:1213–1220. <https://doi.org/10.1002/zaac.202000438>
- Zhao JY, Ren N, Zhang JJ (2021) Lanthanide complexes with 2,6-dimethylbenzoic acid and 2,2':6',2''-terpyridine: Crystal structures, thermochemical property and luminescent behavior. *Thermochim Acta* 699:178915. <https://doi.org/10.1016/j.tca.2021.178915>
- Zhao QQ, Ren N, Zhang JJ (2018) Syntheses, crystal structures, luminescence and thermal properties of three lanthanide complexes with 2-bromine-5-methoxybenzoate and 2,2':6',2''-terpyridine. *Polyhedron* 144:1–5. <https://doi.org/10.1016/j.poly.2017.12.036>
- Zhou MX, Ren N, Zhang JJ (2021) Crystal Structure, Thermal decomposition mechanism and properties of lanthanide supramolecular complexes based on 2,4,6-trimethylbenzoic acid and 5,5'-dimethyl-2,2'-bipyridine. *Acta Phys.-Chim. Sin* 37:2004071–2004080. <https://doi.org/10.3866/PKU.WHXB202004071>
- Zong GC, Huo JX, Ren N, Zhang JJ, Qi XX, Gao J, Geng LN, Wang SP, Shi SK (2015) Preparation, characterization and properties of four new trivalent lanthanide complexes constructed using 2-bromine-5-methoxybenzoic acid and 1,10-phenanthroline. *Dalton Trans* 44:14877–14886. <https://doi.org/10.1039/c5dt01969a>

Publisher's Note Springer Nature remains neutral with regard to jurisdictional claims in published maps and institutional affiliations.